A feasibility study of a molecular-based patient setup verification method using a parallel-plane PET system

Satoshi Yamaguchi[1], Masayori Ishikawa[1], Satoshi Tanabe[1], Gerard Bengua[2], Kenneth Sutherland[1], Teiji Nishio[3], Naoki Miyamoto[1], Ryusuke Suzuki[2], Hiroki Shirato[4]

[1]Department of Medical Physics and Engineering, Hokkaido University Graduate School of Medicine, N-15 W-7 Kita-ku Sapporo, 060-8638 Japan

[2]Department of Medical Physics, Hokkaido University Hospital, N-14 W-5 Kita-ku Sapporo, 060-8648 Japan

[3]Particle Therapy Division, Research Centre for Innovative Oncology, National Cancer Centre, Kashiwa, 6-5-1 Kashiwano-ha, Kashiwa-shi, Chiba, 277-8577 Japan

[4]Hokkaido University Graduate School of Medicine, N-15 W-7 Kita-ku Sapporo, 060-8638 Japan

Abstract

A feasibility study of a novel PET-based molecular image guided radiation therapy (m-IGRT) system was conducted by comparing the PET-based registration with radiographic registration. We selected a pair of opposing parallel-plane PET system for the practical implementation. Five different sizes of ^{18}F cylindrical sources (diameter: 8, 12, 16, 24, 32 mm) were used to determine setup errors. PET data acquisition times were 1, 3 and 5 min. Image registration was performed by 5 observers. Setup errors from the PET system were compared with setup errors from image intensifier-based fluoroscopy. The in-plane and cross-plane FWHM of the profile of a 2 mm diameter sources for the parallel-plane PET system were approximately 1.8 mm and 8.1 mm, respectively. The majority of the mean registration errors obtained from the PET-based registration were not significantly different from those obtained from the radiographic registration. Acquisition time did not appear to result in significant differences in the mean registration error. The mean registration error for the PET-based registration was found to be 0.93±0.33 mm. This is not statistically different from the radiographic registration which had mean registration error of 0.92±0.27 mm. Our results suggest that m-IGRT is feasible for clinical use with a parallel plane PET-based registration.

1. Introduction

Image guided radiotherapy (IGRT) techniques are presently used clinically to improve the accuracy of treatment delivery in photon radiation therapy. IGRT is used to correct for patient positioning errors prior to or during treatment by using image guided procedures. Patient setup can be verified through the co-registration of digitally reconstructed radiographs (DRR) and imaging plate (IP) or electronic portal imaging device (EPID) images taken using MV-X rays from a linear accelerator (Linac) while the patient is set up just prior to treatment (Dong et al 1995, Gilhuijs et al 1996). Linac systems with on-board cone-beam computed tomography (CBCT) devices have also been developed (Pouliot et al 2005, Jaffray et al 2002, Groh et al 2002, Ford et al 2002, Munbodh et al 2006). CBCT allows the imaging of the target volume and organs at risk during treatment. Accuracy of patient setup verification error is important in order to ensure that the actual treatment geometry is as close as possible to the treatment planning geometry. At present, patient setup verification is done mostly by the alignment of bony structures in radiographic images taken during treatment and those used for treatment planning. The change in the tumour size and location inside the body is usually difficult to determine during treatment. Making the tumour visible in the irradiation field is thus desirable in order to improve setup verification accuracy.

Positron emission tomography (PET) based on sugar metabolism in the tumour caused by ^{18}F-fluorodeoxyglucose (FDG) uptake has been shown to be effective for distinguishing the tumour for diagnosis (Som et al 1980). Since PET images are functional images, they allow cell activity to be visible, thus the tumour position can be determined. Another promising radioactive tracer for PET imaging is ^{18}F-fluoromisonidazole (FMISO) (Nehmeh et al 2008). FMISO is able to delineate hypoxic cells, which are known to be radiation resistant, in tumours. Clinical trials have demonstrated improved tumour control by delivering escalated doses to hypoxic tumour cells using IMRT and other techniques (Lee et al 2008).

The spatial resolution and sensitivity of recent PET devices have also been significantly improved. This has been partly due to (1) the development of new detector elements such as BGO or GSO crystals, (2) the change in the acquisition method from 2D to 3D, and (3) the invention of depth-of-interaction (DOI) (Wienhard et al 2002, Yamaya et al 2003). The application of PET technology as a new modality for diagnostic procedures is also now being considered; for example, positron emission mammography (PEM) (Smith et al 2003, Huesman et al 2000, Zhang et al 2007, Ralyman et al 2008, MacDonald et al 2009). In this study, we propose a PET-based molecular image guided radiation therapy (m-IGRT) system for patient setup verification in cases where significant tumour shrinkage or growth may occur, such as intracranial or head and neck. In the practical implementation of an m-IGRT system, it is preferable that the PET device is combined with a radiotherapy gantry to guarantee mechanical precision. There are, however, some restrictions on how the PET detectors can be mounted to the present

radiotherapy gantries.

Because PET is a device that detects the annihilation radiation caused by positrons, it is necessary that at least a pair of opposed detectors are arranged to detect the two photons simultaneously. It is preferable that the isocenter of the pair of opposed detectors is identical to the isocenter of the radiotherapy unit. A structure with a wide open space between a pair of opposed detectors is also needed so that the irradiation field used to treat does not become obstructed. The gantry rotation of the radiotherapy unit and the movement or the rotation of the couch must also be considered. Moreover, it is necessary to secure a wide field of view to use the device for setup verification. However, it is difficult in the conventional PET detector geometry, with ring-shape arrangement, to achieve this purpose. We therefore selected a geometry with a pair of opposing parallel-plane detectors. The advantage of this detector geometry is that it is structurally simple, and that it can be mounted easily on a radiotherapy gantry, similar to on-board imaging (OBI) devices.

In order to evaluate the feasibility of molecular image guided registration, we used the Beam On-Line PET system (BOLPs), developed at the National Cancer Centre East hospital in Japan (Nishio et al 2005, 2006, 2010). The system consists of a pair of opposing parallel-plane detectors mounted on the gantry which can detect annihilation radiation produced by positron emitters (e.g., ^{15}O, ^{14}O, ^{13}N and ^{11}C). BOLPs was originally developed for visualizing irradiation fields by measuring the activity of positron emitters which are generated by nuclear reactions from incident proton beams. The BOLPs has the same detector configuration as our proposed system.

In this paper, we report on the feasibility of a novel m-IGRT by comparing the PET-based registration with radiographic registration.

2. Materials and Method

2.1. Beam On-Line PET system

The BOLPs at the National Cancer Centre East hospital in Japan was used to verify the accuracy of patient setup verification with our proposed parallel-plane PET system. The BOLPs detector is mounted at the gantry of the proton irradiation system as shown in figure 1(a). The detector head consists of 3,960 BGO crystals (2 mm × 2 mm × 20 mm) covering a 16 × 16 cm^2 field of view. The distance between the detector heads was fixed at 40 cm. Shown in figure 1(b) are the two reference planes, the cross-plane and in-plane, used in the evaluation of the full-width at half-maximum (FWHM) of the profile of a 2 mm diameter source. The FWHM of the profile is indicative of the spatial resolution.

The BOLPs also includes an on-board X-ray system that allows the acquisition of radiographic images for patient setup verification. We compared the accuracy of image registration using radiographic-based and PET-based registration.

2.2. Image reconstruction method

The detector configuration of the BOLPs is different from conventional PET systems in that they do not encircle the subject. Due to the parallel placement of the detector heads, there is limited angular sampling and loss of line of response (LOR) and the usual sinogram-based reconstruction method is not applicable. Therefore, the maximum likelihood-expectation maximization (MLEM) method (Shepp and Vardi 1982) was used in the LOR-based reconstruction using Siddon's algorithm (Siddon 1985).

In this study, only the detector sensitivity correction was applied while ignoring the other possible correction factors to account for scattering or absorption.

2.3. Phantom configuration

Two custom-made phantoms were used in our measurements. The first phantom was a polycarbonate cylindrical phantom with a width of 20 cm and a diameter of 18 cm. We refer to this phantom as the *cylindrical phantom.* It contained 13 radiation point sources (each with a diameter of about 2 mm) that were arranged as shown in figure 2. The other phantom was a polycarbonate plate containing 5 cylindrical radiation sources of various diameters (i.e., 8, 12, 16, 24, 32 mm) with 1.5cm depth, representing different tumour sizes as shown in figure 3(a). This was attached to an acrylic slab (height: 20 cm, width: 18.5 cm, depth: 0.3 cm) as shown in figure 3(b). In this paper, we refer to this phantom setup as the *tumour phantom*. The radiation sources in both the cylindrical phantom and tumour phantom used ^{18}F that was homogeneously mixed in a gelatinous medium.

2.4. FWHM of the profile of a 2 mm diameter sources

The unique detector geometry of the BOLPs does not allow the use of the filtered back projection reconstruction as specified in the National Electrical Manufactures Association (NEMA) standard which is used for the evaluation of PET detectors. Therefore we used a modified method for image reconstruction based on PEM (Smith et al 2004, MacDonald et al 2009), which has a detector geometry similar to the BOLPs. PEM devices and the BOLPs have anisotropic spatial resolutions because the detectors do not encircle the object and the detectors do not rotate to acquire the full 360º angular sampling required for full 3-dimensional tomography. Parallax error caused by the thickness of scintillation crystals is considered (Hoffman et al 1989, Larches et al 2005).

We evaluated the FWHM of the profile using the cylindrical phantom shown in figure 2 for the cylindrical-shaped radiation sources using a width of 2 mm and a diameter of 2 mm. The ^{18}F activity was 40 kBq/ml. The projection data was measured for 15 minutes at a gantry angle of 0 degree. The image reconstruction via the MLEM method was applied with the pixel size and slice thickness of 1.00 mm and a reconstruction volume of 15 × 15 × 15 cm^3. The 13 point sources were expressed as FWHM of the profile curve at each position.

2.5. Registration experiments

2.5.1 PET-based registration

PET-based registration was performed by comparing the in-plane image reconstructed by the BOLPs and the image obtained from a conventional PET (Discovery ST, General Electric, Schenectady, New York). The pixel size and slice thickness were 3.91 mm and 3.27 mm, respectively. We placed the tumour phantom in a conventional PET such that the polycarbonate plate was parallel to the longitudinal axis and the centre of the plate aligned with the isocenter. Data collection was performed for 15 minutes.

The tumour phantom was then placed at the isocenter of the BOLPs to obtain the data for the in-plane image and measured by the BOLPs. Data were also collected for two additional conditions where the tumour phantom was displaced by 2 mm and 7 mm along the y-axis, away from the isocenter to avoid observer's bias from trial learning. Each measurement with the BOLPs was carried out for 5 minutes. The activity of the ^{18}F was 20 kBq/ml and the background activity was 4 kBq/ml. The gantry angle was fixed at 0 degree. MLEM image reconstruction was applied with the pixel size and slice thickness of 1.00 mm and a reconstruction volume of 15 × 15 × 5 cm^3. In-plane images corresponding to 1, 3 and 5 min measurements were reconstructed for each setup position. Image registration based on the in-plane image at the isocenter for each setup position was performed by 5 observers. The reference image was reconstructed from a conventional PET image.

2.5.2 Radiographic registration

To compare the accuracy of radiographic-based and PET-based registration, we also performed image registration using images obtained from an x-ray CT and a fluoroscope system. The tumour phantom was placed at the isocenter of the x-ray CT following the same set-up used in the PET measurement. The pixel size and slice thickness were 0.98 mm and 1.25 mm, respectively. Fluoroscope images of the tumour phantom were also taken using the installed fluoroscopic system in the proton irradiation system. The position of the tumour phantom was subsequently moved along the y-axis to take additional data at 2 mm and 7 mm from the isocenter. The reference image used in the radiographic registration was the DRR re-constructed from x-ray CT.

2.5.3 Registration accuracy evaluation

To evaluate the accuracy of the registration methods, image registration trials using an in-house software were performed for 10 trials. Each trial consisted of 5 different images shown twice to the observers. Five observers estimated the shifts in each trial. From the image registration data, we calculated the registration error (RE) using Eq. (1). Actual shift (Y_{actual}) was 0, 2 and 7 mm along the Y-axis. Z_{obs} and Y_{obs} in the equation refer to the observed translation along the Z-axis and Y-axis performed by the 5 subjects respectively. Statistical analysis was performed based on the registration error for both the

radiographic-based and PET-based registration.

$$RE\ (\text{mm}) = \sqrt{(Z_{obs})^2 + (Y_{obs} - Y_{actual})^2} \ldots Eq.(1)$$

RE : Registration error

Z_{obs} : Observed translation along to Z-axis

Y_{obs} : Observed translation along to Y-axis

Y_{actual} : Actual setup couch translation along to Y-axis (0, 2, 7 mm)

2.5.4 Statistical analysis

Statistical analysis of our data was performed using JMP 8 (SAS Institute Inc.) software. The mean registration error and standard deviation (SD) for the various tumour diameters were determined based on acquisition time for data collection (i.e., 1 min, 3 min and 5 min) and modality (BOLPs, x-ray fluoroscopy). Data were analyzed by one-way ANOVA, while the differences among means were analyzed by two-sided Student's t test with the level of statistical significance set to $p<0.05$.

3 Results

3.1. FWHM of the profile of a 2 mm diameter sources

Figure 4 shows the reconstructed in-plane and cross-plane images of the cylindrical phantom corresponding to a gantry angle of 0 degree. The reconstructed source diameter at the central position was larger than the others due to blurring caused by adjacent sources. The FWHM of each radiation source is shown in figure 5. The mean ± SD for FWHM was 1.8 ± 0.3 mm in the in-plane image, 8.1 ± 1.2 mm in the cross-plane image at a gantry angle of 0 degree.

3.2. Registration accuracy evaluation

Shown in figure 6 are the reconstructed in-plane images of the tumour phantom at a gantry angle of 0 degree. Images from left to right correspond to the three acquisition times (1, 3 and 5 min) for data collection while those from top to bottom correspond to the positions of the phantom (0, 2 and 7 mm) during data acquisition. Gray-scale window level of the images was adjusted to enhance the contrast. The measured activity at the tumour increased linearly as a function of acquisition time, and contrast to the background was constant and any inconsistency was not observed among three positions.

Figure 7 shows the variations in the observed PET-based and radiographic-based registration errors with respect to acquisition time, phantom position and tumour diameter. PET-based registration is given by the PET-BOLPs data (1, 3 and 5 min) and radiographic-based registration by the DRR-portal (X-ray) data. Dependence of registration error on phantom position was not seen among each tumour diameter.

Shown in table 1 is the mean ± SD of the registration error based on our ANOVA analysis. For the tumour diameter of 8 mm the mean registration error of the PET-BOLPs image registration appears to be influenced by the acquisition time with the longest acquisition time having the least mean registration error. The registration error for the DRR-portal image registration was comparable to that of the shortest acquisition time of 1 min for the PET-BOLPs. The differences in the registration error between the image registration modalities listed in table 1 for the 8 mm tumour diameter was found to be significant at a p-value of <0.0001. On the other hand, the mean registration error in all four cases for the tumour diameter of 12 mm were found to be statistically insignificant (p=0.3545) with their mean registration error ranging between 0.49 and 0.63. For tumour diameters of 16 mm and 24 mm, the three acquisition times using PET-BOLPs resulted in similar registration errors and a relatively smaller registration error for the DRR-portal image registration. However, the difference between the PET-BOLPs and DRR-portal was found to be statistically significant only for the 24 mm tumour at p=0.0003. A significant difference between the PET-BOLPs and DRR-portal image registration errors were obtained for the 32 mm diameter tumour.

The statistical comparisons of the mean registration error and SD for each tumour (radioactive source) diameter obtained from the PET-BOLPs registration at 1 min, 3 min, and 5 min and the DRR-portal image registration are shown in figure 8 and figure 9.

For the tumour diameter of 8 mm, the differences in the registration error for the three acquisition times used in the PET-BOLPs registration were found to be statistically significant. However, when compared to the registration error of the DRR-portal image registration, only the 5 min PET-BOLPs data yielded a significant difference. The mean registration errors for the image registration conditions shown in figure 8(b) and 8(c) for tumour diameters of 12 mm and 16 mm were not statistically different.

However, a larger variation in the computed registration error was observed for the 16 mm tumour.

For the tumour diameter of 24 mm, the mean registration error obtained for the DRR-portal image registration was found to be significantly smaller compared to those obtained using the PET-BOLPs registration method. Furthermore, acquisition time did not appear to result in significant differences in the mean registration error of the PET-BOLPs registration. Like those of the results for the 8 mm-tumour, the mean registration error of 32 mm-tumour decreased with acquisition time in the PET-BOLPs registration.

A comparison of the registration error SDs is shown in figure 9 for the various tumour diameters and data acquisition methods. The SDs for most of the results were not statistically different. The image registration SDs of the PET-BOLPs with 3-minute acquisition was statistically same as the DRR-portal image registration.

4. Discussion

The over-all evaluation of the accuracy of PET-based registration independent of the tumour size is

necessary. We therefore performed a comparative study of the registration error obtained with PET-BOLPs and DRR-portal image registrations for a number of hypothetical tumour sizes. The cumulative mean registration error and SD for five different tumour sizes using four registration conditions (i.e., PET-BOLPs at 1, 3 and 5 min acquisition time and DRR-portal image registration) are shown in figure 10. A general trend of decreasing mean RE and SD for longer acquisition time is seen for the PET-BOLPs registration. The 3 min data acquisition in the BOLPs yielded comparable results to radiographic-based registration while the 5 min acquisition appears to result in lower registration error.

Our tumour phantom experiments show that the mean of registration error for PET-BOLPs is approximately 0.93 mm and the standard deviation is approximately 0.33 mm. This is not statistically different from the DRR-portal registration which had mean registration error of 0.92±0.27 mm

Although there are no reports on the accuracy of image registration using molecular imaging, there have been a number of publications regarding the accuracy between DRR and EPID image registration. Dong et al (1995) showed that the phantom studies demonstrated that the correlation procedure had a standard deviation of 0.5 mm in aligning translational shifts. Gilhuijs et al (1996) registered 2D portal images with CT data, and their automatic 3D analysis of patient set-up accuracy was about 1 mm for translation. In the clinical case, Hurkmans et al (2001) reports setup errors less than 2.0 mm (1SD) for head and neck, 2.5 mm (1 SD) for prostate, 3.0 mm (1 SD) for general pelvic, 3.5 mm (1 SD) for lung cancer. It is also reported that the set-up verification accuracy varies widely, depending on the treatment site, method of immobilization and institution. The registration error for PET-BOLPs was lower than previously reported radiographic registrations. This could be due to the fact that the image registration was performed with tumour parts itself, not with the skeletal structure, or that there was a phantom dependency. Nevertheless, the registration error for PET-BOLPs image registration was not significantly different to DRR-portal image registration in our experiments. As shown in figure 10(b), the registration error is dependent on the data acquisition time. In order to apply PET-based registration clinically, the acquisition time should be taken into account. Longer acquisition time will result in lower registration error but it will cause patient discomfort. Optimum acquisition time needs to be considered while maintaining the registration accuracy. However, this is complicated because it depends on the tumour and normal tissues uptake and radiation attenuation in the patient's body. Patient immobilization may also be necessary in order to minimize the effects of inter- and intra-fraction motion caused by patient movement. The effect of respiratory induced motion should be considered in future work.

If FDG is used as the tracer in PET-based registration, it will also be uptaken in normal organs such as the brain, liver, kidneys, bladder etc. This will be a problem in this image registration modality. However, because of the high spatial resolution of our parallel-plane PET system along the in-plane direction, it should be possible to distinguish the tumour FDG uptake from the adjacent normal organs which also accumulate FDG.

Conventional radiographic registration is performed in both LR and AP directions for setup verification.

Registration in two directions is also preferable in PET-based molecular image guided systems. Additionally, this high spatial resolution will likewise be useful in hypoxic region imaging using FMISO because the hypoxic region distribution in the tumour is complex (Nehmeh et al 2008).

5. Conclusion

We performed a basic study of the accuracy of image registration using the PET-based molecular image guided method. Phantom experiments showed that there is no significant difference between radiographic-based and PET-based registration. Our results suggest that m-IGRT is feasible for clinical use with a parallel plane PET-based registration. Furthermore, the system will provide additional information for image registration when bony structures cannot be recognized with radiography.

Acknowledgments

This research was a part of the "Innovation COE Program for Future Drug Discovery and Medical Care" project and partially supported by the Grant-in-Aid for Special Coordination Funds for Promoting Science and Technology of the Japanese Ministry of Education, Culture, Sports, Science and Technology.

References

Dong L, Boyer A L 1995 An image correlation procedure for digitally reconstructed radiographs and electronic portal images *Int. J. Radiat. Oncol. Biol. Phys.* **33** 1053–60

Ford E C et al 2009 18F-FDG PET/CT for image-guided and intensity-modulated radiotherapy *J. Nucl. Med* . **50** 1655-65

Ford E C, Chang J, Mueller K, Sidhu K, Todor D, Mageras G, Yorke E, Ling C C and Amols H 2002 Cone-beam CT with megavoltage beams and an amorphous silicon electronic portal imaging device: potential for verification of radiotherapy of lung cancer *Med. Phys.* **29** 2913–24

Gilhuijs K G A, van de Ven P J H and van Herk M 1996 Automatic three-dimensional inspection of patient setup in radiation therapy using portal images, simulator images, and computed tomography data *Med. Phys.* **23** 389–99

Groh B A, Siewerdsen J H, Drake D G, Wong J W and Jaffray D A 2002 A performance comparison of flat-panel imager-based MV and kV cone-beam CT *Med. Phys.* **29** 967–75

Hoffman E J et al 1989 PET system calibrations and corrections for quantitative and spatially accurate images *IEEE Trans. Nucl. Sci.* **36** 1108-12

Huesman R H et al 2000 List-mode maximum-likelihood reconstruction applied to positron emission mammography (PEM) with irregular sampling *IEEE Trans. Med. Imaging.* **19** 532-7

Hurkmans C W et al 2001 Set-up verification using portal imaging; review of current clinical practice *Radiother Oncol.* **58** 105-20

Jaffray D A, Siewerdsen J H, Wong J W and Martinez A A 2002 Flat-panel cone-beam computed tomography for image-guided radiation therapy *Int. J. Radiat. Oncol. Biol. Phys.* **53** 1337–49

Lee N Y, Le Q T 2008 New developments in radiation therapy for head and neck cancer: intensity-modulated radiation therapy and hypoxia targeting *Semin Oncol.* **35** 236-50

Lerche C W et al 2005 Depth of γ-ray interaction within continuous crystals from the width of its scintillation light-distribution *IEEE Trans. Nucl. Sci.* **52** 560-72

MacDonald L et al 2009 Clinical Imaging Characteristics of the Positron Emission Mammography Camera: PEM Flex Solo II *J. Nucl. Med.* **50** 1666-75

Munbodh R, Jaffray D A, Moseley D J, Chen Z, Knisely J P S, Cathier P and Duncan J S 2006 Automated 2D–3D registration of a radiograph and a cone beam CT using line-segment enhancement *Med. Phys.* **33** 1398–411

Nehmeh S A et al 2008 Reproducibility of intratumor distribution of 18F-fluoromisonidazole in head and neck cancer *Int. J. Radiat. Oncol. Biol. Phys.* **70** 235-242

Nishio T et al 2005 Distributions of β+ decayed nuclei generated in the CH2 and H2O targets by the target nuclear fragment reaction using therapeutic MONO and SOBP proton beam *Med. Phys.* **32** 1070-82

Nishio T et al 2006 Dose-volume delivery guided proton therapy using beam online PET system *Med. Phys.* **33** 4190-7

Nishio T et al 2010 The development and clinical use of a beam on-line pet system mounted on a rotating gantry port in proton therapy *Int. J. Radiat. Oncol. Biol.Phys.***76** 277–86

Park S L et al 2008 Evaluation of the combined effects of target size, respiratory motion and background activity on 3D and 4D PET/CT images *Phys. Med. Biol.* **53** 3661–79

Pouliot J et al 2005 Low-dose megavoltage cone-beam CT for radiation therapy *Int. J. Radiat. Oncol. Biol. Phys.* **61** 552–60

Raylman R R et al 2008 The positron emission mammography/tomography breast imaging and biopsy system (PEM/PET): design, construction and phantom-based measurements *Phys. Med. Biol.* **53** 637–53

Shepp L A, Vardi Y 1982 Maximum likelihood reconstruction for emission tomography IEEE Trans. *Med Imaging.* **1** 113-22

Siddon R L 1985 Fast calculation of the exact radiological path for a three dimensional CT array *Med. Phys.* **12** 252–5

Smith M F et al 2003 Analysis of Factors Affecting Positron Emission Mammography (PEM) Image Formation *IEEE Trans. Nucl. Sci.* **50** 53-9

Smith M F et al 2004 Positron emission mammography with tomographic acquisition using dual planar detectors: initial evaluations *Phys. Med. Biol.* **49** 2437–52

Som P et al 1980 A Fluorinated Glucose Analog, 2-fluoro-2-deoxy-D-glucose (F-18): Nontoxic Tracer for

Rapid Tumor Detection *J Nucl Med.* **21** 670-5

Sorcini B, Tilikidis A 2006 Clinical application of image-guided radiotherapy, IGRT (on the Varian OBI platform) *Cancer Radiother.* **10** 252-7

Verellen D et al 2003 Quality assurance of a system for improved target localization and patient set-up that combines real-time infrared tracking and stereoscopic X-ray imaging *Radiother. Oncol.* **67** 129–41

Wienhard K et al 2002 The ECAT HRRT: performance and first clinical application of the new high resolution research tomograph *IEEE Trans. Nucl. Sci.* **49** 104–10

Yamaya T, Hagiwara N, Obi T, Yamaguchi M, Kita K, Ohyama N, Kitamura K, Hasegawa T, Haneishi H and Murayama H 2003 DOI-PET image reconstruction with accurate system modeling that reduces redundancy of the imaging system *IEEE Trans. Nucl. Sci.* **50** 1404–9

Zhang J et al 2007 Study of the performance of a novel 1 mm resolution dual-panel PET camera design dedicated to breast cancer imaging using Monte Carlo simulation *Med. Phys.* **34** 689-702

Figures and Tables

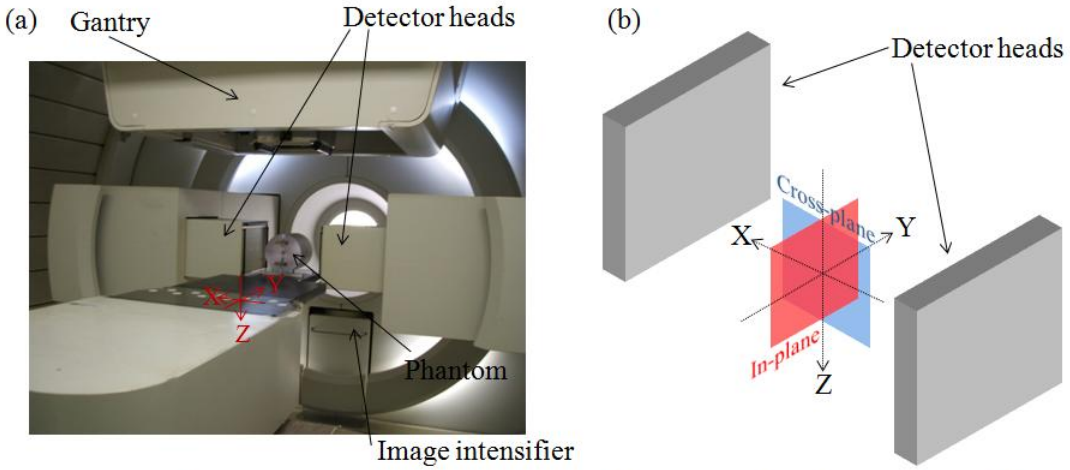

Figure 1. (a) Beam On-Line PET system and (b) Illustration of in-plane and cross-plane where gantry angle is at 0 degree.

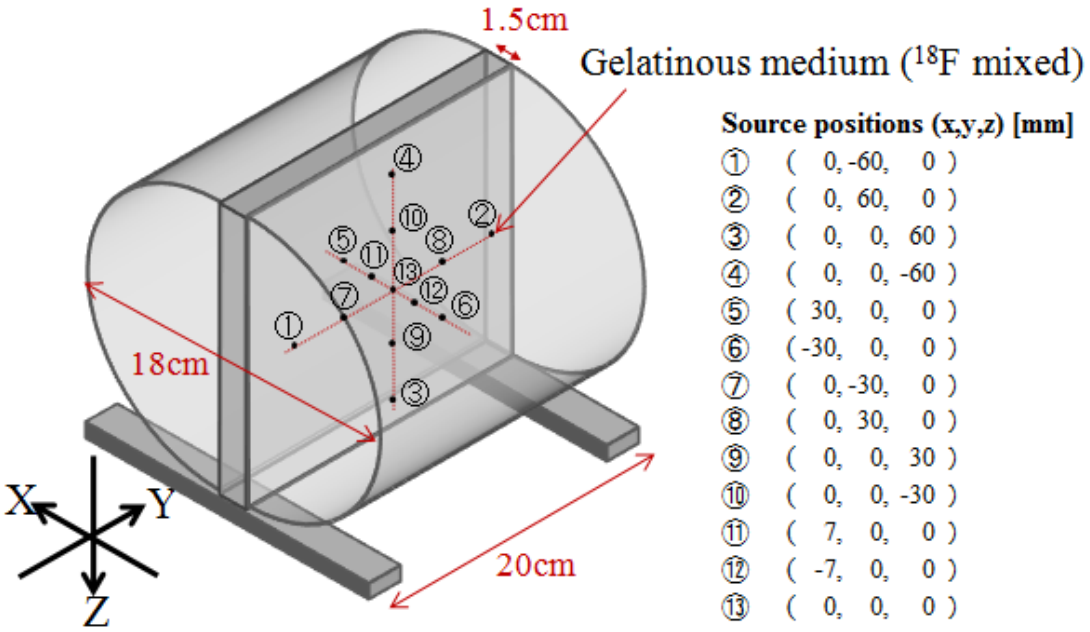

Figure 2. Cylindrical phantom with sources placed in the positions as indicated.

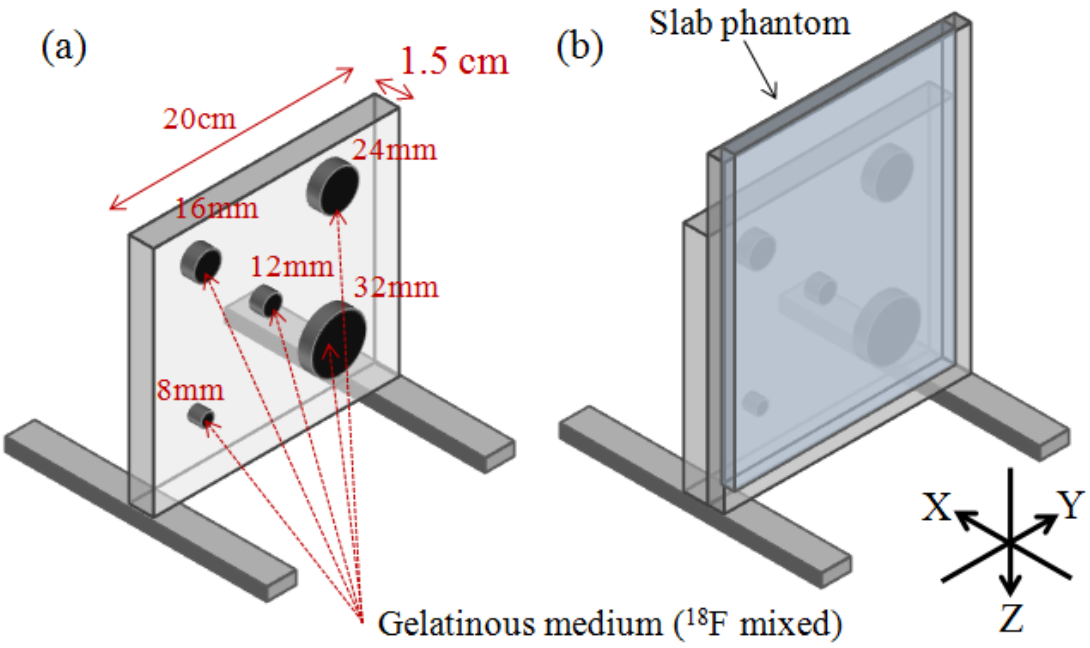

Figure 3. (a) Polycarbonate plate containing sources of various diameters representing different tumour sizes. (b) The plate in (a) attached to a acrylic slab phantom.

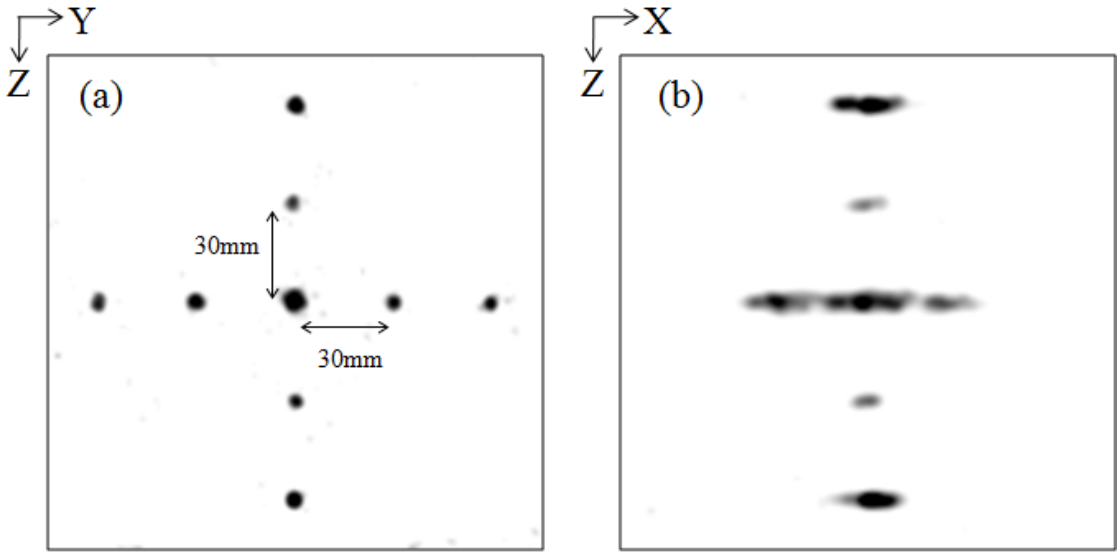

Figure 4. Reconstructed (a) in-plane and (b) cross-plane images of the point sources corresponding to gantry angle of 0 degree.

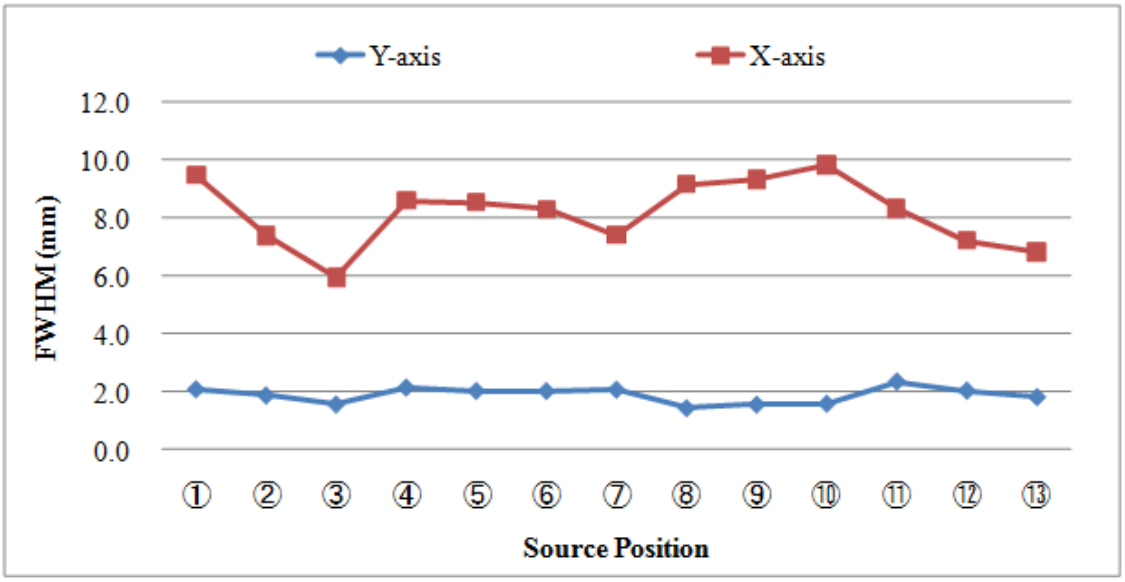

Figure 5. FWHM of the profile of a 2 mm diameter source obtained from the cylindrical phantom in figure 2.

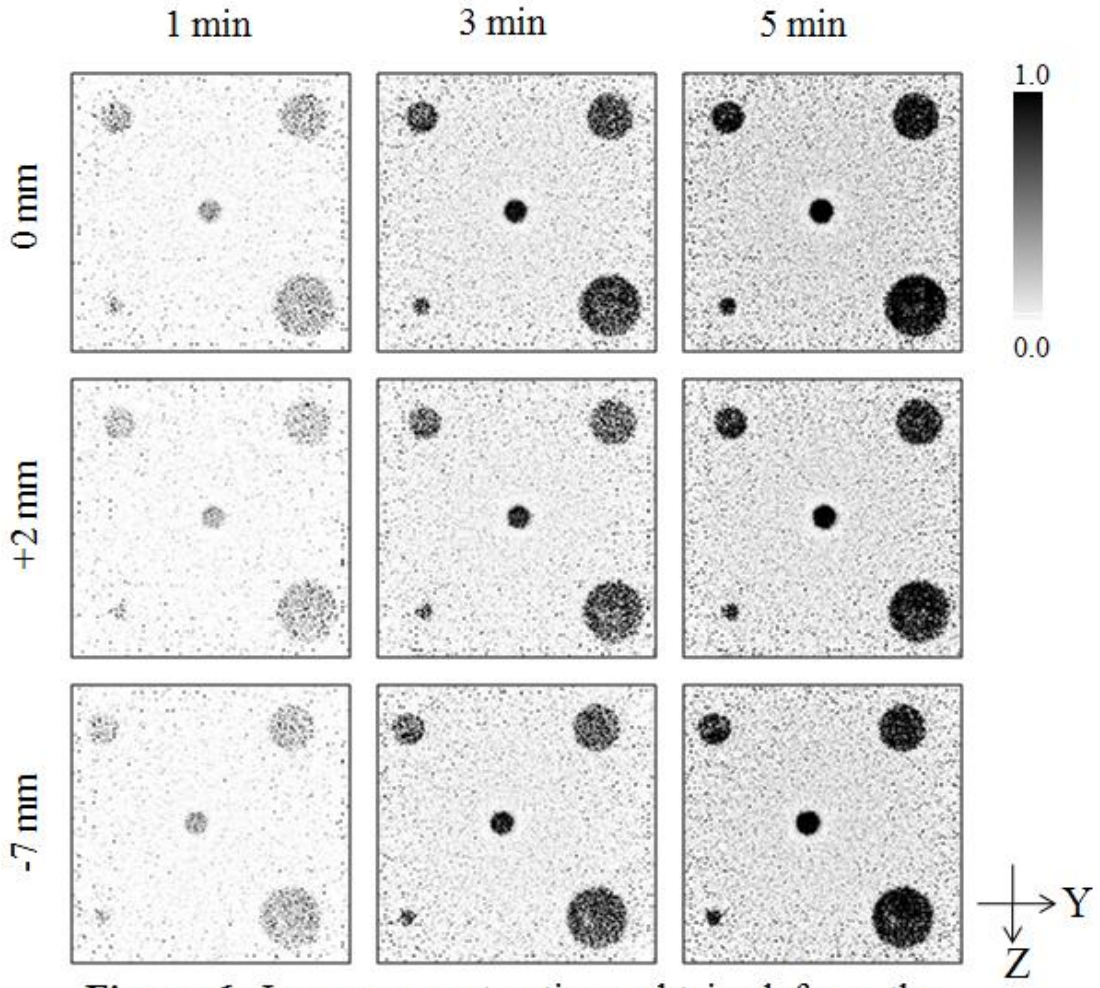

Figure 6. Image reconstructions obtained from the tumour phantom in figure 3(b). Shown are the results for three phantom positions relative to the isocenter and at an acquisition time of 1 min, 3 min and 5 min, respectively.

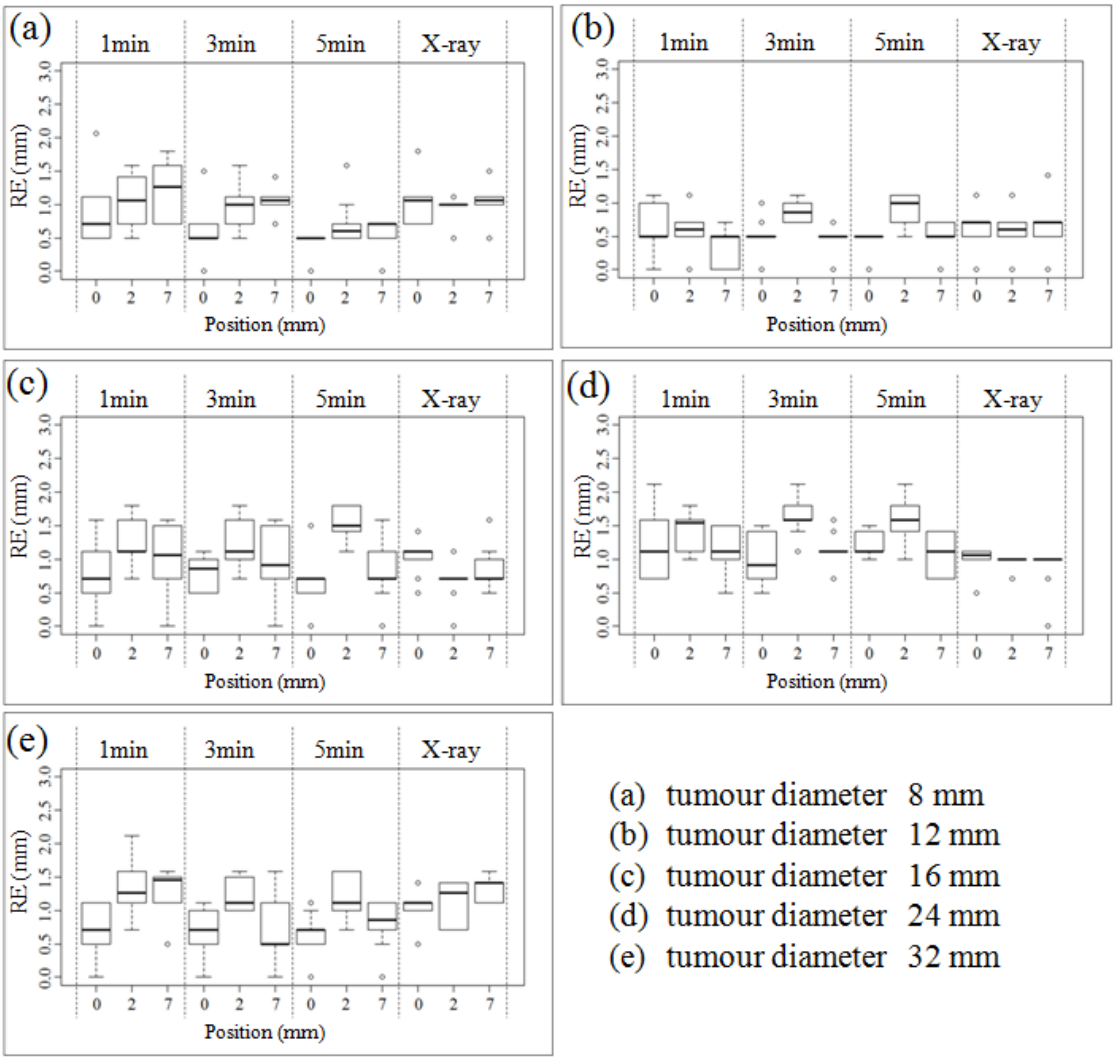

Figure 7. Registration error in the tumour phantom of figure 3(b). Shown are the results for three phantom positions relative to the isocenter(0), isocenter+2mm(2) and isocenter+7mm(7) at an acquisition time of 1 min, 3 min and 5 min, respectively.

Table 1. Statistical comparison of registration error using ANOVA at an acquisition time of PET-BOLPs (1 min, 3 min and 5 min), and DRR-portal (X-ray) image.

	Tumour diameter				
Case	8mm	12mm	16mm	24mm	32mm
PET-BOLPs (1min)	1.07 ± 0.42	0.49 ± 0.34	1.02 ± 0.44	1.28 ± 0.35	1.12 ± 0.39
PET-BOLPs (3min)	0.87 ± 0.29	0.59 ± 0.24	1.01 ± 0.38	1.25 ± 0.29	0.86 ± 0.37
PET-BOLPs (5min)	0.56 ± 0.26	0.60 ± 0.24	1.00 ± 0.34	1.30 ± 0.26	0.88 ± 0.32
DRR-portal (X-ray)	0.98 ± 0.28	0.63 ± 0.30	0.87 ± 0.31	0.95 ± 0.20	1.17 ± 0.26
(p-value)	<.0001*	0.3545	0.522	0.0003*	0.0044*

* Significant ($p<0.05$).

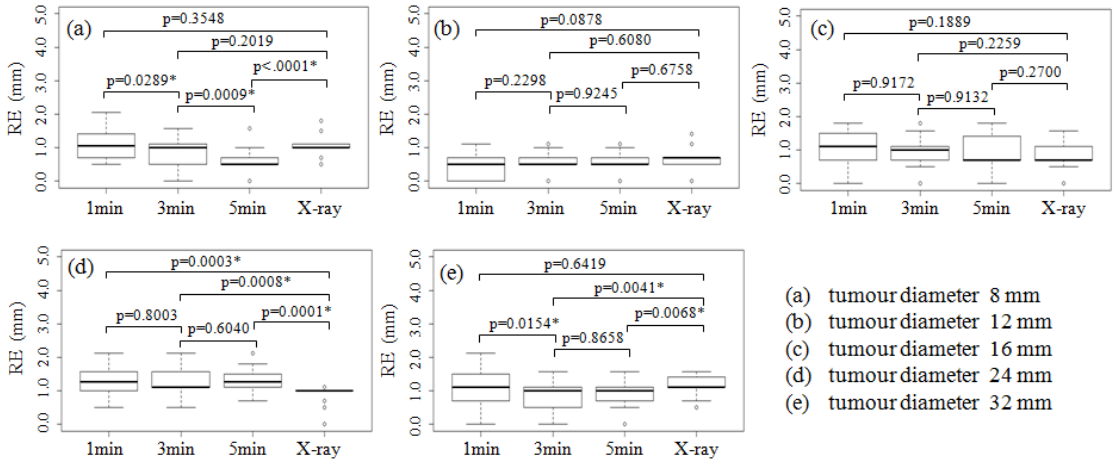

Figure 8. Statistical comparison of the mean registration error for the five tumour diameter evaluated (i.e., 8, 12, 16, 24 and 32 mm) using the Student's t-test at $p < 0.05$ significance level.

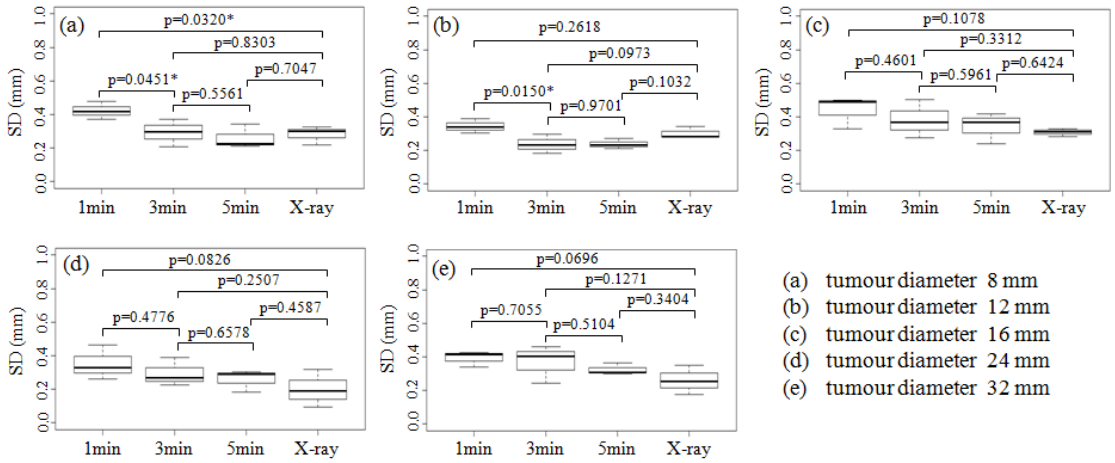

Figure 9. Statistical comparison of the standard deviation of the mean registration error for the five tumour diameter evaluated (i.e., 8, 12, 16, 24 and 32 mm) using the Student's t-test at $p < 0.05$ significance level.

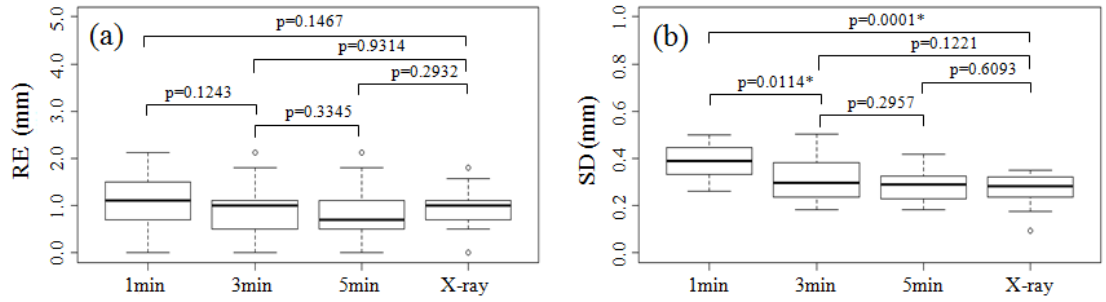

Figure 10. Statistical comparison of (a) the mean registration error and (b) the standard deviation for an over-all evaluation using the Student's t test at $p<0.05$ significance level.